

Structures associated with the Borromean rings complement in the Poincaré ball

Anton A. Nazarenko[†] and A.V. Nazarenko[‡]

[†]*Faculty of Mechanics and Mathematics, Taras Shevchenko National University of Kyiv,
UA-01601 Kyiv, Ukraine
anton.nazarenko02@gmail.com*

[‡]*Bogolyubov Institute for Theoretical Physics of NAS of Ukraine,
UA-03143 Kyiv, Ukraine
nazarenko@bitp.kyiv.ua*

Abstract

Guided by physical needs, we deal with the rotationally isotropic Poincaré ball, when considering the complement of Borromean rings embedded in it. We consistently describe the geometry of the complement and realize the fundamental group as isometry subgroup in three dimensions. Applying this realization, we reveal normal stochastization and multifractal behavior within the examined model of directed random walks on the rooted Cayley tree, whose six-branch graphs are associated with dendritic polymers. According to Penner, we construct the Teichmüller space of the decorated ideal octahedral surface related to the quotient space of the fundamental group action. Using the conformality of decoration, we define six moduli and the mapping class group generated by cyclic permutations of the ideal vertices. Intending to quantize the geometric area, we state the connection between the induced geometry and the sine-Gordon model. Due to such a correspondence we obtain the differential two-form in the cotangent bundle.

Keywords: Borromean rings complement; fundamental group; Cayley tree; random walk; decorated Teichmüller space; sine-Gordon equation

1 Introduction

Numerous physical problems require their formulation in isotropic three-dimensional space, an example of which is the Poincaré unit ball model with its own group of isometries, including three-dimensional rotations. The hyperbolicity of the latter implies the consideration of geometric structures with a negative Euler characteristic, which determines the number of topological degrees of freedom, also used for physical modeling. Here we focus on the complement of Borromean rings (BRC), which represent the simplest Brunnian link [1], and some of the structures associated with it. In studying them, we adhere to the chosen space model, although the often used Klein model is mathematically convenient due to its group of $SL(2, \mathbb{C})$ isometries [2, 3, 4].

Dealing with the basic homotopy groups of the link and decorated Teichmüller space [5], we goal to provide a framework suitable for further use in physics¹. It is due to associating the Borromean rings with quantum entanglement [6, 7], Efimov trimers [8, 9], polymers [10], as well as for the development of quantum geometry, i.e. finding the spectra of quantized

¹We are forced to omit here a detailed review of many works devoted to the study and use of Borromean rings, but note some areas of their appearance.

geometric characteristics [11] and/or using the quantum groups [12]. The last point, in our opinion, is of conceptual importance, and therefore the research begun here looks promising.

Having implemented the fundamental group generated by three-dimensional parabolic generators, the problem of symmetrization of functions with respect to the group operation naturally arises [3]. In this regard, we consider the Cayley tree embedded in the Poincaré ball and rooted at the origin to formulate the partition function of the directed random walk model related to polymer physics [13]. Defining this function up to N th generation, we expect rapid stochastization of the terms of the Poincaré-type series and the revelation of multifractality. The sought multifractal exponents are appropriate for comparing different models and allow interpretation in the spirit of statistical physics [14]. Besides, resorting to Markov chains to compute characteristics is similar to using a mean field approximation.

We also focus on the deformations (classes) of conformal structures induced on the surface of a regular hyperbolic octahedron, the ideal vertices of which are fixed by the parabolic generators. Using the realized group as a marking, we involve the decorated Teichmüller space and its mapping class group operating through vertex permutations. Decorating implies the inclusion of horospheres centered at the vertices and obtaining curves of their intersection with octahedron faces, always orthogonal to the corresponding edges of the octahedron [5]. Then conformality is ensured by the conservation of right angles regardless of the size of the horospheres [15, 16], when the horosphere size is changed by hyperbolic boost [5].

In order to determine a differential two-form needed for further geometry quantization, we search a connection with a suitable dynamical model. It can be realized by relating the angular size of each intersection curve and the hyperbolic distance from it to the origin in order to reveal the kink of the sine-Gordon model [17]. This should allow us to induce the differential two-form within the Hamiltonian formalism, as well as construct algebra of geometric quantities in the future. We admit the applicability of this strategy to developing quantum geometry [18, 19] and field theory [20].

The paper is organized as follows. In Sec. 2, we describe the geometry of the complement of Borromean rings in the Poincaré ball and implement the fundamental group as its isometry subgroup. Multifractal exponents of a directed random walk model on the Cayley tree are studied in Sec. 3 using numerical and approximate methods. In Sec. 4, we study the structure of the decorated Teichmüller space and its mapping class group. Introducing the moduli, we connect the induced geometry and the sine-Gordon model. We finish our considerations with the Discussion.

2 Geometry and symmetry of the Borromean rings complement

2.1 Spaces and their isometries

Let us define the spaces and their symmetries that we shall use. According to Thurston's arguments [1], good knots and links induce a hyperbolic structure in the three-dimensional space where they naturally exist. Denote by \mathcal{H}_3 the three-dimensional manifold embedded in \mathbb{R}^3 and equipped with a hyperbolic metric of constant negative curvature. It is useful to split \mathcal{H}_3 into hyperplanes and complexify them:

$$\mathcal{H}_3 \ni x = (x_1, x_2, x_3) \mapsto (x_1 + ix_2, x_3) = (z, t) \in \mathbb{C} \times \mathbb{R}. \quad (1)$$

Thus, fixing the hyperplane $t = 0$, we require that the resulting two-dimensional manifold $\mathcal{H}_2 \ni z \simeq (z, 0)$ inherits the hyperbolic structure (\simeq denotes isomorphic equivalence).

This (orthogonal) projection becomes apparent by considering the two Poincaré models: unit ball $\mathbb{B} = \{x \in \mathbb{R}^3 \mid \|x\|_{\mathbb{B}}^2 = x_1^2 + x_2^2 + x_3^2 < 1\} \simeq \mathcal{H}_3$ and unit disc $\mathbb{D} = \{z \in \mathbb{C} \mid \|x\|_{\mathbb{D}}^2 = |z|^2 < 1\} \simeq \mathcal{H}_2$. Their infinitesimal intervals $ds_{\mathbb{B},\mathbb{D}}^2$ and distances $\text{dist}_{\mathbb{B},\mathbb{D}}$ are given by the common formulas:

$$ds_{\mathbb{B},\mathbb{D}}^2 = 4 \frac{\|dx\|_{\mathbb{B},\mathbb{D}}^2}{(1 - \|x\|_{\mathbb{B},\mathbb{D}}^2)^2}, \quad (2)$$

$$\text{dist}_{\mathbb{B},\mathbb{D}}(x, y) = 2 \operatorname{arcsinh} \frac{\|x - y\|_{\mathbb{B},\mathbb{D}}}{\sqrt{(1 - \|x\|_{\mathbb{B},\mathbb{D}}^2)(1 - \|y\|_{\mathbb{B},\mathbb{D}}^2)}}. \quad (3)$$

These are also generalized for n dimensions and lead to the Gaussian curvature $K = -1$.

Geodesics in \mathbb{B} and \mathbb{D} are either diameters passing through the origin or arcs orthogonally intersecting the boundaries $\partial\mathbb{B}$ and $\partial\mathbb{D}$. To give the geodesic $\mathbf{r}(\theta)$ connecting two points with radius-vectors $\mathbf{r}_1, \mathbf{r}_2 \in \mathbb{B}$, we suggest the parametrization:

$$\begin{aligned} \mathbf{r}(\theta) &= \mathbf{r}_0 + (\mathbf{r}_1 - \mathbf{r}_0) \cos \theta + [\mathbf{n} \times (\mathbf{r}_1 - \mathbf{r}_0)] \sin \theta, \quad \mathbf{r}(0) = \mathbf{r}_1; \\ \mathbf{r}_0 &= \frac{\mathbf{n} \times \mathbf{m}}{|\mathbf{r}_1 \times \mathbf{r}_2|}, \quad \mathbf{n} = \frac{\mathbf{r}_1 \times \mathbf{r}_2}{|\mathbf{r}_1 \times \mathbf{r}_2|}, \quad \mathbf{m} = c_2 \mathbf{r}_1 - c_1 \mathbf{r}_2, \quad c_i = \frac{\mathbf{r}_i^2 + 1}{2}. \end{aligned} \quad (4)$$

In fact, (4) describes a circular arc with center at \mathbf{r}_0 and radius $R = |\mathbf{r}_1 - \mathbf{r}_0| = |\mathbf{r}_2 - \mathbf{r}_0| = \sqrt{\mathbf{r}_0^2 - 1}$; \mathbf{n} is the normal to the circle plane covering three points $\mathbf{r}_1, \mathbf{r}_2$, and the origin $\mathbf{r} = 0$ that do not lie on the same straight line. The equation $|\mathbf{r}(\theta_2) - \mathbf{r}_2| = 0$ defines the parameter θ_2 , and one has (numerically) that

$$\text{dist}_{\mathbb{B}}(\mathbf{r}_1, \mathbf{r}_2) = 2R \int_0^{\theta_2} \frac{d\theta}{1 - \mathbf{r}^2(\theta)}. \quad (5)$$

Let us first turn to $\mathcal{H}_2 \simeq (\mathbb{D}, ds_{\mathbb{D}}^2)$ for our geometry and group constructions. It implies the use of an orientation-preserving subgroup of isometries $\text{Isom}(\mathbb{D})$ that preserve $ds_{\mathbb{D}}^2$, that is, $PSU(1, 1) \simeq SU(1, 1)/\{\pm 1\}$, whose element g acts freely on $z \in \mathbb{D}$ via a linear-fractional transformation:

$$g[z] = \frac{uz + v}{\bar{v}z + \bar{u}}, \quad g = \begin{pmatrix} u & v \\ \bar{v} & \bar{u} \end{pmatrix}, \quad \det g = |u|^2 - |v|^2 = 1. \quad (6)$$

Then, having obtained a matrix representation of some group $\Gamma \subset PSU(1, 1)$, we need to extend the action of its generators $g = (g_{i,j})$ up to the ball \mathbb{B} :

$$g[(z, t)] = (z_g(z, t), t_g(z, t)), \quad g[(z, 0)] = (g[z], 0), \quad (7)$$

such that $\text{dist}_{\mathbb{B}}(x, y) = \text{dist}_{\mathbb{B}}(x_g, y_g)$ for $x = (z_1, t_1)$, $y = (z_2, t_2)$, and their images $x_g = (z_g(z_1, t_1), t_g(z_1, t_1))$, $y_g = (z_g(z_2, t_2), t_g(z_2, t_2))$. In general, this can be done using explicit formulas, for example, from [21].

For our purposes, starting with parabolic generators of $PSU(1, 1)$:

$$g = \begin{pmatrix} 1 + ia & -ia e^{i\varphi} \\ ia e^{-i\varphi} & 1 - ia \end{pmatrix}, \quad g[e^{i\varphi}] = e^{i\varphi}, \quad a, \varphi \in \mathbb{R}, \quad (8)$$

when g^n is simply obtained by means of replacement $a \mapsto na$, we write down the extended action of $g[\mathbf{r}]$ for $\mathbf{r} \equiv (x \ y \ t)^T \in \mathbb{B}$ in terms of the linear combinations:

$$\xi_1 = x \sin \varphi - y \cos \varphi, \quad \xi_2 = y \sin \varphi + x \cos \varphi; \quad x^2 + y^2 = \xi_1^2 + \xi_2^2. \quad (9)$$

Thus, we derive that

$$g \left[\begin{pmatrix} x \\ y \\ t \end{pmatrix} \right] = \frac{1}{a^2[t^2 + (\xi_2 - 1)^2] + (a\xi_1 + 1)^2} \begin{pmatrix} \tilde{x} \\ \tilde{y} \\ t \end{pmatrix}, \quad (10)$$

$$\tilde{x} = x + (a^2 \cos \varphi + a \sin \varphi)[\xi_1^2 + (\xi_2 - 1)^2 + t^2] + 2a\xi_1 \cos \varphi,$$

$$\tilde{y} = y + (a^2 \sin \varphi - a \cos \varphi)[\xi_1^2 + (\xi_2 - 1)^2 + t^2] + 2a\xi_1 \sin \varphi.$$

It serves to get the group $\Gamma_* \subset \text{Isom}(\mathbb{B})$ from Γ . Obviously, Γ_* based on Γ cannot take into account all symmetries of three-dimensional objects. Therefore, additional generators of $\text{Isom}(\mathbb{B})$ should be introduced, by operating, for example, with $SO(3)$ rotations due to the spherical symmetry supposed.

Indeed, the Rodrigues' formula [22] allows us to present the rotation of \mathbf{r} by an angle φ around the direction along the unit vector \mathbf{n} as

$$R_{\mathbf{n},\varphi}[\mathbf{r}] = \mathbf{r} \cos \varphi + \mathbf{n}(\mathbf{n} \cdot \mathbf{r})(1 - \cos \varphi) + [\mathbf{n} \times \mathbf{r}] \sin \varphi. \quad (11)$$

It is such that $R_{\mathbf{n},\varphi}^{-1} = R_{\mathbf{n},-\varphi}$; $R_{\mathbf{m},\varphi} = R R_{\mathbf{n},\varphi} R^{-1}$ for $\mathbf{m} = R[\mathbf{n}]$ and rotation R .

At the end, we also note the HNN group extension [23] and the Möbius transformations in terms of quaternions [24] (see also references therein).

2.2 The Borromean rings complement

Let us consider the link which is formed by Borromean rings and sketched in Fig. 1(left), and define the symmetry of its complement. This link is isotopically equivalent to the braid in Fig. 1(right), where the ends of each strand are closed.

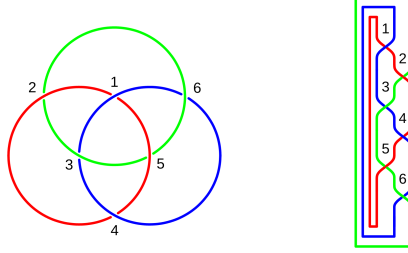


Figure 1: Left panel: Sketch of Borromean rings. There are *seven* intrinsic triangles formed by intersections, namely (123), (135), (156), (126), (234), (345), (456), and *one* extrinsic triangle (246). Right panel: The closed braid with a top-to-bottom direction. There is a group relation $(\sigma_2 \sigma_1^{-1})^3 = 1$ in terms of crossings σ_1 (between red and blue strands) and σ_2 (between blue and green ones).

As was argued by Thurston [1], the Borromean rings complement (BRC) is a hyperbolic three-manifold M that has a tessellation consisting of two ideal regular octahedra. The group G of isometries of M acts freely and transitively on the set of flags of this tessellation, and it has to be of the order 48.

We start from considering the ideal regular octahedron in Fig. 2 with ideal vertices at $\pm \mathbf{i}$, $\pm \mathbf{j}$, $\pm \mathbf{k}$, where $\{\mathbf{i}, \mathbf{j}, \mathbf{k}\}$ is the standard basis of \mathbb{R}^3 . Its edges are the twelve geodesic arcs within the ball, see (4).

The octahedron basis in \mathbb{D} is stabilized by the parabolic generators of the group $\Gamma = \langle h_1, h_2 \mid (h_1 h_2)^2 = -I \rangle$, where

$$h_1 = \begin{pmatrix} 1 - i & -1 \\ -1 & 1 + i \end{pmatrix}, \quad h_2 = \begin{pmatrix} 1 - i & -i \\ i & 1 + i \end{pmatrix}. \quad (12)$$

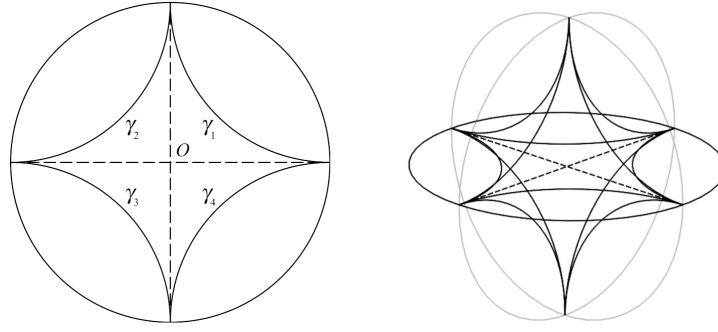


Figure 2: Left panel: Basis of a hyperbolic octahedron with ideal vertices in \mathbb{D} plane. Right panel: Centered hyperbolic octahedron in \mathbb{B} .

Defining $h_3 = h_2 h_1 h_2^{-1}$ and $h_4 = h_1^{-1} h_2 h_1$ so that $(h_2 h_3)^2 = (h_3 h_4)^2 = (h_1 h_4)^2 = h_4 h_3 h_2 h_1 = -I$, every generator h_k ($k = \overline{1, 4}$) fixes the point $z_k = \exp(i\pi k/2) \in \partial\mathbb{D}$ and determines the mapping $h_k : \gamma_k \rightarrow \gamma_{k+1}$ ($\gamma_5 = \gamma_1$) in Fig. 2(left). As we shall see below, the extensions of h_k connect also the vertical edges of the octahedra whose bases lie in \mathbb{D} . However, in order to fill the entire ball \mathbb{B} with octahedra, additional tools are needed. In fact, the group Γ should be extended up to Γ_* by including generators (85)-(92).

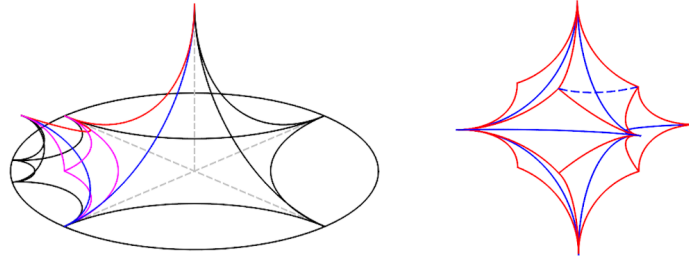


Figure 3: Left panel: Upper parts of two adjacent octahedra. The colored edges of daughter octahedron bound the tetrahedron, which should be glued to the nearest face of the central octahedron. The red and blue edges of tetrahedron in the third quadrant of \mathbb{D} are identified with the colored edges of the central octahedron by using h_2^{-1} and h_3 , respectively. Right panel: The red-edge dodecahedron covers the central octahedron with blue edges. This is obtained by taking eight tetrahedra along the equatorial perimeter of the central octahedron and then gluing them to its eight faces. Dashed geodesic smoothly connects the nearby finite vertices of glued tetrahedra.

As it was previously argued [25], gluing two octahedra together to obtain BRC, the maximally symmetrical body that can be produced is the rhombic *dodecahedron*, which inherits the octahedral symmetry of the order 48. To achieve it, we may cut one octahedron into eight tetrahedra with further gluing of each to the eight faces of another octahedron. We are implementing this by using Γ_* .

First, acting by the four generators h_k on the (edges of) octahedron in Fig. 2(right), four daughter octahedra are obtained with bases in four quadrants of \mathbb{D} . The new octahedra are geodesic solids in $(\mathbb{B}, ds_{\mathbb{B}}^2)$, whose vertical edges (and faces) with $t \neq 0$ are resulted due to (10). By construction, daughter octahedra have only one edge adjacent to the parent octahedron, see Fig. 3(left).

Further, we extract tetrahedra from a daughter octahedron by cutting it with three hyperplanes of octahedral symmetry. Such an operation is shown in Fig. 3(left). Each

tetrahedron has right dihedral angles at the vertex in the center of the octahedron.

In our approach, we glue one face of the adjacent tetrahedron to the face of the central octahedron, as shown in Fig. 3(left). This is allowed due to the geodesic nature of faces and edges of equal areas and lengths. Seemingly, the procedure of cutting four daughter octahedra with taking two tetrahedra (in the upper and lower hemisphere) seems easier than decomposing one octahedron (with basis in \mathbb{D}) into eight tetrahedra with subsequent manipulations. Anyway, this is also admissible using h_k . As a result, all procedures lead to the rhombic dodecahedron (with eight finite vertices at points $(\pm 1/3 \pm 1/3 \pm 1/3)^\top$), which specifies the complement and is shown in Fig. 3(right). Thereby, we complete the BRC geometrical description using Γ and Γ_* .

2.3 BRC group realization

Let us now realize the BRC fundamental group $\pi_1(\text{BRC})$ that is the semi-direct product $\mathbb{Z}_2^3 \rtimes \mathcal{C}_3$, where \mathcal{C}_3 is the third-order cyclic group [26, 27]. This is subgroup of the group $G \simeq \mathbb{Z}_2^3 \rtimes S_3$ of three-manifold M with symmetric group S_3 acting transitively on the standard basis of the vector space \mathbb{Z}_2^3 .

Having specified the parent octahedron Oct as shown in Fig. 2, the action of \mathbb{Z}_2^3 on either octahedra of the tessellation of M corresponds to the reflections in the coordinate hyperplanes of \mathbb{B} . Besides, the elementary group \mathbb{Z}_2^3 acts trivially on the set Y of cusps of M , while the quotient group $G^Y = S_3$ acts transitively on Y .

We adopt the Wirtinger representation of $\Gamma_{\text{BRC}} = \langle g_1, g_2, g_3 \mid R_1, R_2, R_3 \rangle$:

$$\begin{aligned} R_1 &: (g_2^{-1} g_3 g_2 g_3^{-1}) g_1 = g_1 (g_2^{-1} g_3 g_2 g_3^{-1}), \\ R_2 &: (g_3^{-1} g_1 g_3 g_1^{-1}) g_2 = g_2 (g_3^{-1} g_1 g_3 g_1^{-1}), \\ R_3 &: (g_1^{-1} g_2 g_1 g_2^{-1}) g_3 = g_3 (g_1^{-1} g_2 g_1 g_2^{-1}). \end{aligned} \quad (13)$$

Note that the known $SL(2, \mathbb{C})$ matrix realizations are in [2, 3, 4].

We have already stabilized the Oct in $(\mathbb{B}, ds_{\mathbb{B}}^2)$ by a subgroup of $\text{Isom}(\mathbb{B})$ with the *functions composition* as group operation. Now, we are interested in realization $\varphi : \pi_1(\text{BRC}) \mapsto \text{Isom}(\mathbb{B})$ which implies the mapping $g_i \mapsto \varphi(g_i)$.

We start with the generators of three Abelian subgroups in terms of “meridians” and “longitudes” for three fixed points:

$$\tilde{h}_1^m h_1^n = h_1^n \tilde{h}_1^m, \quad \tilde{h}_2^m h_2^n = h_2^n \tilde{h}_2^m, \quad \tilde{h}_+^m h_+^n = h_+^n \tilde{h}_+^m; \quad n, m \in \mathbb{Z}. \quad (14)$$

They transform $\mathbf{r} = (x \ y \ t)^\top \in \mathbb{B}$ so that their composition reads $h_i h_j[\mathbf{r}] = h_i[h_j[\mathbf{r}]]$.

Indeed, every pair (h_k, \tilde{h}_k) is Abelian if the parabolic h_k and \tilde{h}_k have the same fixed point in $\partial\mathbb{B}$. The needed generators can easily be obtained by using $SO(3)$ rotation (11). We have collected the auxiliary generators in Appendix A.

In principle, (14) means that we have six generators, and we would like to reduce their number to three by imposing extra relations (13).

Selecting generators from Appendix A, we obtain the realization Γ_{BRC} operating in \mathbb{B} :

$$\begin{aligned} g_1^n \left[\begin{pmatrix} x \\ y \\ t \end{pmatrix} \right] &= \frac{1}{n^2[x^2 + (y-1)^2] + (nt-1)^2} \begin{pmatrix} y-1 + n^2[x^2 + (y-1)^2] + (nt-1)^2 \\ t - n[x^2 + (y-1)^2 + t^2] \end{pmatrix}, \\ g_2^n \left[\begin{pmatrix} x \\ y \\ t \end{pmatrix} \right] &= \frac{1}{n^2[t^2 + (x+1)^2] + (ny-1)^2} \begin{pmatrix} x+1 - n^2[t^2 + (x+1)^2] - (ny-1)^2 \\ y - n[(x+1)^2 + y^2 + t^2] \end{pmatrix}, \\ g_3^n \left[\begin{pmatrix} x \\ y \\ t \end{pmatrix} \right] &= \frac{1}{n^2[y^2 + (t-1)^2] + (nx+1)^2} \begin{pmatrix} x + n[x^2 + y^2 + (t-1)^2] \\ t-1 + n^2[y^2 + (t-1)^2] + (nx+1)^2 \end{pmatrix}, \end{aligned} \quad (15)$$

where n is an exponent.

It is seen that g_1 , g_2 , and g_3 fix the points $(0 \ 1 \ 0)^\top$, $(-1 \ 0 \ 0)^\top$, $(0 \ 0 \ 1)^\top$, respectively. Due to (11) we have that $g_1 = R_{\mathbf{j},\pi/2} h_1^{-1} R_{\mathbf{j},-\pi/2}$, $g_2 = h_2$, and $g_3 = R_{\mathbf{i},\pi/2} h_1^{-1} R_{\mathbf{i},-\pi/2}$, while $g_2^{-1} g_3 g_2 g_3^{-1} = h_1^2$, $g_3^{-1} g_1 g_3 g_1^{-1} = R_{\mathbf{i},\pi/2} h_2^{-2} R_{\mathbf{i},-\pi/2}$, and $g_1^{-1} g_2 g_1 g_2^{-1} = R_{\mathbf{j},\pi/2} h_2^{-2} R_{\mathbf{j},-\pi/2}$.

The easiest way to get other realizations of the group Γ_{BRC} is to rotate these generators altogether around the main coordinate axes as $\tilde{g}_k = R_{\mathbf{n},\pi/2} g_k R_{\mathbf{n},-\pi/2}$, where vector \mathbf{n} is one of $\{\mathbf{i}, \mathbf{j}, \mathbf{k}\}$.

3 Cayley tree and multifractality

One of the direct applications of the group Γ_{BRC} is a random walk model on the generated Cayley tree. Such a statistical model can be used in dendritic polymer physics [13] for example. It represents an alternative to two-dimensional models using hyperbolic generators. As an advantage, the multifractal indices calculated here are easily compared with the others.

3.1 Construction of the Cayley tree and spectrum analysis

Using the realization (15), let us enumerate the generating set of Γ_{BRC} as

$$\{\gamma_i \mid i = \overline{1, 6}\} = \{g_1, g_2, g_3, g_1^{-1}, g_2^{-1}, g_3^{-1}\}. \quad (16)$$

By associating the points \mathbb{B} with their radius-vectors and considering the origin $\mathbf{0}$ as the root point, the six-branch Cayley tree of the N th generation is defined as embedded in the ball \mathbb{B} and formed by the set of $6 \times 5^{N-1}$ admissible graphs that sequentially connect the vertices:

$$\gamma_{i_1}[\mathbf{0}], \gamma_{i_2} \gamma_{i_1}[\mathbf{0}], \dots, \gamma_{i_N} \gamma_{i_{N-1}} \dots \gamma_{i_1}[\mathbf{0}]; \quad i_t \in \{1, 2, 3, 4, 5, 6\}. \quad (17)$$

An admissible graph with the word $\{i_N, i_{N-1}, \dots, i_1\}$ is allowed by the conditional probability $p_N(i_N, i_{N-1}, \dots, i_1) = 1$ which we define as

$$p_N(i_N, i_{N-1}, \dots, i_1) = \prod_{t=2}^N p_2(i_t, i_{t-1}), \quad p_2(i_t, i_{t-1}) = \begin{cases} 0, & |i_t - i_{t-1}| = 3 \\ 1, & \text{otherwise} \end{cases}. \quad (18)$$

It is easy to see that p_N prohibits backward steps and makes the graph directed. Besides, there is the relation:

$$\sum_{i_1=1}^6 \dots \sum_{i_N=1}^6 p_N(i_N, i_{N-1}, \dots, i_1) = v(N), \quad v(N) = 6 \times 5^{N-1}, \quad (19)$$

where $v(N)$ is the number of vertices of N th generation. This means that the Cayley tree of the N th generation is a rooted pencil of $v(N)$ branches (with common parts).

Strictly speaking, the compositions of the original generators (16) give us the resulting transformations of all types: parabolic, elliptic, hyperbolic. It is naively expected that only combinations of the form γ_i^n ($n \in \mathbb{Z}$) and those represented in the brackets of relations (13) remain parabolic. These features add interest to the study of the (finite) Cayley tree. In this regard, we turn to the multifractal analysis.

Our study is based on the N th generation partition function of moment order q :

$$\mathcal{Z}_N(q) = \sum_{i_1=1}^6 \dots \sum_{i_N=1}^6 p_N(i_N, i_{N-1}, \dots, i_1) e^{q\mathcal{L}(i_N, i_{N-1}, \dots, i_1)}, \quad (20)$$

$$\mathcal{L}(i_N, i_{N-1}, \dots, i_1) = \sum_{t=1}^N \text{dist}_{\mathbb{B}}(\mathbf{0}, \gamma_{i_t} \gamma_{i_{t-1}} \dots \gamma_{i_1}[\mathbf{0}]). \quad (21)$$

Mathematically, the function $\mathcal{Z}_N(q)$ is a kind of Poincaré series over a group. Physically, (20) can be interpreted as the Feynman integral of the Boltzmann weight over discrete paths, associating the parameter q with the inverse temperature $1/T$, which takes positive and negative values. At the same time, the form of functional \mathcal{L} should actually provide a second-order phase transition, the geometric analogue of which is multifractal behavior. Here, (21) may be considered as the perimetric characteristic of a surface consisting of adjacent triangles connecting the root point and two points of different generations. Also note that similar functions were previously used in [28] for a Fuchsian group operating in $(\mathbb{D}, ds_{\mathbb{D}}^2)$.

From forthcoming analysis it is easily seen that the functional

$$\mathcal{L}^0(i_N, i_{N-1}, \dots, i_1) = \sum_{t=1}^N \text{dist}_{\mathbb{B}}(\gamma_{i_{t-1}} \dots \gamma_{i_1}[\mathbf{0}], \gamma_{i_t} \gamma_{i_{t-1}} \dots \gamma_{i_1}[\mathbf{0}]) \quad (22)$$

does not lead to multifractal behavior because of the vanishing variance of the \mathcal{L}^0 -spectrum. However, such a term may also be involved elsewhere.

Since there are $v(N)$ admissible values of (21), they can be enumerated with a single index ζ : $\{\mathcal{L}_{\zeta} \mid \zeta = 1, v(N)\} = \{\mathcal{L}(\{i_t\}) \mid p_N(\{i_t\}) = 1\}$, to reduce $\mathcal{Z}_N(q)$ to

$$\mathcal{Z}_N(q) = \sum_{\zeta=1}^{v(N)} e^{q\mathcal{L}_{\zeta}}; \quad \mathcal{Z}_N(0) = v(N). \quad (23)$$

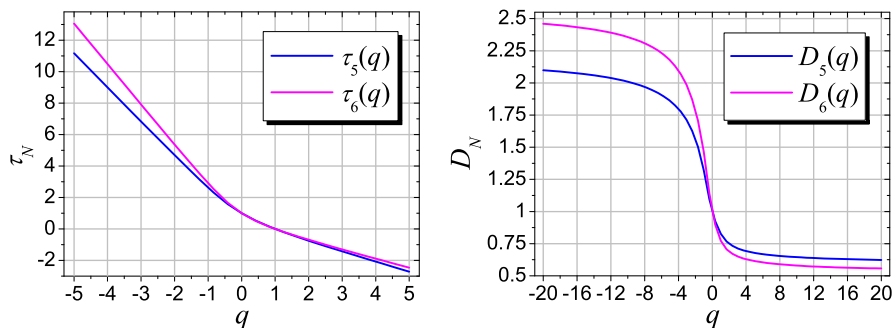


Figure 4: Mass spectrum τ_N (left panel) and spectrum of fractal dimensions D_N (right panel) as functions of moment order q for different generations N .

According to the recipe in [14], we define the scaling exponent $\tau_N(q)$, sometimes called the mass spectrum, and the spectrum of fractal dimensions $D_N(q)$, associated with the Hausdorff dimensions, up to multiplication by the carrier dimension:

$$\tau_N(q) = \frac{1}{\ln v(N)} [\ln \mathcal{Z}_N(q) - q \ln \mathcal{Z}_N(1)], \quad D_N(q) = \frac{\tau_N(q)}{1 - q}. \quad (24)$$

A comparison of these functions for different N can be done in Fig. 4. As is seen, the slope of the functions to the left of $q = 0$ grows as N increases.

Another important characteristic is the spectrum of singularities $f_N(\alpha_N)$, determined (in parametric form) by using the Legendre transform:

$$f_N(q) = \tau_N(q) - q \frac{d\tau_N(q)}{dq}, \quad \alpha_N(q) = -\frac{d\tau_N(q)}{dq}. \quad (25)$$

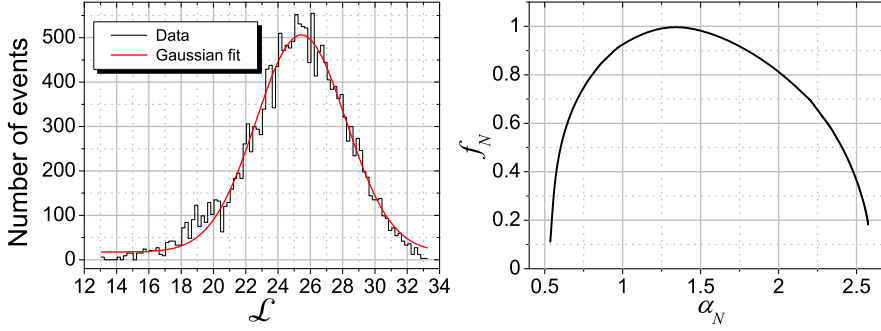


Figure 5: Characteristics of the model for $N = 6$. Left panel: The number of \mathcal{L}_ζ within the intervals $\Delta\mathcal{L} = 0.2$ from $\mathcal{L}_{\min} \simeq 13.04$ to $\mathcal{L}_{\max} \simeq 33.1$. Right panel: The spectrum of singularities $f_N(\alpha_N)$; $\alpha_{N,\min} \simeq 0.5353$ and $\alpha_{N,\max} \simeq 2.574$ for $N = 6$.

By definition, one gets that

$$\alpha_{N,\min} = \lim_{q \rightarrow +\infty} D_N(q), \quad \alpha_{N,\max} = \lim_{q \rightarrow -\infty} D_N(q). \quad (26)$$

The calculated characteristics indicate normal stochastization with increasing N in Fig. 5(left), which also leads to a fairly wide range of the Lipschitz–Hölder exponent α_N in Fig. 5(right) for $N = 6$. Firstly, this means that for large N the central limit theorem (CLT) is applicable [29]. And secondly, a wide range of α shows the absence of a dominant subset of graphs (fractals) and the need to take into account all graphs, albeit approximately, when analytically calculating the function $\mathcal{Z}_N(q)$. This motivates us to use a Markov chain (random walk) in our studies.

3.2 Markov chain approximation

Analyzing (23), we first assume that the spectrum $\{\mathcal{L}_\zeta | \zeta = \overline{1, v(N)}\}$ is degenerate. In other words, there is the set $\{\mathcal{L}_s | s = \overline{1, S(N)}\}$ with $S(N) \leq v(N)$ of unequal quantities. Introducing the degeneracy coefficient w_s for each \mathcal{L}_s , we arrive at

$$\mathcal{Z}_N(q) = \sum_{s=1}^{S(N)} w_s e^{q\mathcal{L}_s}. \quad (27)$$

Determining $\mathcal{L}_{\min}(N)$ and $\mathcal{L}_{\max}(N)$ such that $\mathcal{L}_{\min}(N) \leq \mathcal{L}_s \leq \mathcal{L}_{\max}(N)$, the next step is the transition to a continuous limit:

$$\mathcal{Z}_N(q) = v(N) \int_{\mathcal{L}_{\min}(N)}^{\mathcal{L}_{\max}(N)} W_N(\mathcal{L}) e^{q\mathcal{L}} d\mathcal{L}. \quad (28)$$

Taking into account observations from Fig. 5(left), we conclude that the distribution $W_N(\mathcal{L})$ for large N is approximated by a Gaussian:

$$W_N(\mathcal{L}) = A_N \exp \left[-\frac{(\mathcal{L} - \bar{\mathcal{L}}_N)^2}{2\sigma_N^2} \right], \quad \int_{\mathcal{L}_{\min}(N)}^{\mathcal{L}_{\max}(N)} W_N(\mathcal{L}) d\mathcal{L} = 1. \quad (29)$$

Simple calculations result in the approximate (Gaussian) expression:

$$\begin{aligned} \mathcal{Z}_N^*(q) &= v(N) \frac{c_N(q)}{c_N(0)} \exp \left(\frac{1}{2} q^2 \sigma_N^2 + q \bar{\mathcal{L}}_N \right), \\ c_N(q) &= \operatorname{erf} \left(\frac{\mathcal{L}_{\max}(N) - \bar{\mathcal{L}}_N - q\sigma_N^2}{\sqrt{2}\sigma_N} \right) + \operatorname{erf} \left(\frac{\bar{\mathcal{L}}_N + q\sigma_N^2 - \mathcal{L}_{\min}(N)}{\sqrt{2}\sigma_N} \right), \end{aligned} \quad (30)$$

where $\operatorname{erf}(x)$ is the error function [30].

Therefore, the use of CLT allows us to reduce the problem to finding four parameters $\mathcal{L}_{\min}(N)$, $\mathcal{L}_{\max}(N)$, $\bar{\mathcal{L}}_N$, and σ_N that characterize the spectrum $\{\mathcal{L}_\zeta \mid \zeta = \overline{1, v(N)}\}$. In fact, this approximation permits to reproduce the exponent $\tau_N(q)$ for large N and relatively small $|q|$. Then we are left with the task of obtaining analytical estimates $\mathcal{L}_{\min}^*(N)$, $\mathcal{L}_{\max}^*(N)$, $\bar{\mathcal{L}}_N^*$, and σ_N^* , bypassing the calculation of the spectrum $\{\mathcal{L}_\zeta \mid \zeta = \overline{1, v(N)}\}$. To implement our program, we appeal to a number of general properties.

Obviously, the spectrum $\{\mathcal{L}(i_1 \dots i_{N-1}, i_N) \mid p_N(i_1 \dots i_{N-1}, i_N) = 1\}$ coincides with $\{\mathcal{L}(i_N, i_{N-1} \dots i_1) \mid p_N(i_N, i_{N-1} \dots i_1) = 1\}$ for $i_t = \overline{1, 6}$ and $t = \overline{1, N}$. Besides, let us recall that $\operatorname{dist}_{\mathbb{B}}(\mathbf{0}, \mathbf{r}) = \operatorname{dist}_{\mathbb{B}}(\gamma[\mathbf{0}], \gamma[\mathbf{r}])$ and $\operatorname{dist}_{\mathbb{B}}(\mathbf{0}, \gamma[\mathbf{r}]) = \operatorname{dist}_{\mathbb{B}}(\gamma^{-1}[\mathbf{0}], \mathbf{r})$ for $\gamma \in \operatorname{Isom}(\mathbb{B})$.

There is also the triangle rule for the point set $\{\mathbf{0}, \mathbf{r}_{t-1}, \mathbf{r}_t\}$:

$$\begin{aligned} \cosh \operatorname{dist}_{\mathbb{B}}(\mathbf{0}, \mathbf{r}_t) &= \cosh \operatorname{dist}_{\mathbb{B}}(\mathbf{0}, \mathbf{r}_{t-1}) \cosh d_{t,t-1} \\ &\quad + \sinh \operatorname{dist}_{\mathbb{B}}(\mathbf{0}, \mathbf{r}_{t-1}) \sinh d_{t,t-1} \cos \psi_{t,t-1}, \end{aligned} \quad (31)$$

where $d_{t,t-1} = \operatorname{dist}_{\mathbb{B}}(\mathbf{r}_t, \mathbf{r}_{t-1})$; $\psi_{t,t-1}$ is angle opposite to side $(\mathbf{0}, \mathbf{r}_t)$ so that

$$\cos \psi_{t,t-1} = \frac{\mathbf{v} \cdot \mathbf{r}_{t-1}}{|\mathbf{v}| |\mathbf{r}_{t-1}|}, \quad \mathbf{v} = \left. \frac{d\mathbf{r}(\theta)}{d\theta} \right|_{\theta=0}, \quad (32)$$

using (4) for $\mathbf{r}(\theta)$ with $\mathbf{r}_1 = \mathbf{r}_{t-1}$ and $\mathbf{r}_2 = \mathbf{r}_t$.

Evaluating constituents of an admissible $\mathcal{L}(i_1 \dots i_{N-1}, i_N)$, we see that $d_{t,t-1} = \operatorname{dist}_{\mathbb{B}}(\gamma_{i_1} \dots \gamma_{i_{t-1}} \gamma_{i_t}[\mathbf{0}], \gamma_{i_1} \dots \gamma_{i_{t-1}}[\mathbf{0}]) = \operatorname{dist}_{\mathbb{B}}(\gamma_{i_t}[\mathbf{0}], \mathbf{0})$, and we have

$$\ell = \operatorname{dist}_{\mathbb{B}}(\mathbf{0}, \gamma_i[\mathbf{0}]) \simeq 1.762747; \quad i = \overline{1, 6}. \quad (33)$$

Besides, for sufficiently large $\operatorname{dist}_{\mathbb{B}}(\mathbf{0}, \mathbf{r}_t)$ and $\operatorname{dist}_{\mathbb{B}}(\mathbf{0}, \mathbf{r}_{t-1})$ we reduce (31) to

$$\operatorname{dist}_{\mathbb{B}}(\mathbf{0}, \mathbf{r}_t) \simeq \operatorname{dist}_{\mathbb{B}}(\mathbf{0}, \mathbf{r}_{t-1}) + \ln(\cosh \ell + \sinh \ell \cos \psi_{t,t-1}), \quad (34)$$

where the logarithmic term depends on unknown angle $\psi_{t,t-1}$.

In principle, the angle $\psi_{t,t-1}$ depends on \mathbf{r}_{t-1} (and the action of γ_{i_t}), that is, the walk history generated by $\gamma_{i_1}, \dots, \gamma_{i_{t-1}}$. Appealing to the Markov approximation [29] implies neglecting this dependence of the angle on the point. If we replace the logarithmic term in (34) with some $\xi_{i_t, i_{t-1}}$, we get the additive chain:

$$\begin{aligned} \operatorname{dist}_{\mathbb{B}}(\mathbf{0}, \gamma_{i_1}[\mathbf{0}]) &= \ell, \quad \operatorname{dist}_{\mathbb{B}}(\mathbf{0}, \gamma_{i_1} \gamma_{i_2}[\mathbf{0}]) \simeq \ell + \xi_{i_2, i_1}, \\ \operatorname{dist}_{\mathbb{B}}(\mathbf{0}, \gamma_{i_1} \gamma_{i_2} \gamma_{i_3}[\mathbf{0}]) &\simeq \ell + \xi_{i_3, i_2} + \xi_{i_2, i_1}, \quad \text{etc.} \end{aligned} \quad (35)$$

Combining, we arrive at the approximate expression for $p_N(i_1, \dots, i_N) = 1$:

$$\mathcal{L}^*(i_1 \dots i_{N-1}, i_N) = N\ell + \sum_{t=1}^{N-1} (N-t) \xi_{i_{t+1}, i_t}, \quad (36)$$

which depends on the constant 6×6 matrix $\|\xi_{i,j}\|$.

Thus, the \mathcal{L} 's spectrum characteristics can be evaluated as

$$\left\{ \begin{array}{c} \mathcal{L}_{\min}^*(N) \\ \mathcal{L}_{\max}^*(N) \\ \bar{\mathcal{L}}_N^* \end{array} \right\} = N\ell + \frac{N(N-1)}{2} \left\{ \begin{array}{c} \min_{p_2(i,j)=1} (\xi_{i,j}) \\ \max_{p_2(i,j)=1} (\xi_{i,j}) \\ \bar{\xi} \end{array} \right\}, \quad (37)$$

$$(\sigma_N^*)^2 = a_0(N) \left[(\bar{\xi}^2)_0 - \bar{\xi}^2 \right] + 2 \sum_{t=1}^{N-2} a_t(N) \left[(\bar{\xi}^2)_t - \bar{\xi}^2 \right]; \quad (38)$$

$$\bar{\xi} = \frac{1}{v(2)} \sum_{i,j=1}^6 p_2(i,j) \xi_{i,j}, \quad (39)$$

$$(\bar{\xi}^2)_t = \frac{1}{v(2+t)} \sum_{i_1=1}^6 \cdots \sum_{i_{2+t}=1}^6 p_{2+t}(i_1, \dots, i_{2+t}) \xi_{i_2, i_1} \xi_{i_{2+t}, i_{1+t}}, \quad (40)$$

$$a_t(N) = \sum_{s=1}^{N-1-t} s(s+t), \quad a_0(N) + 2 \sum_{t=1}^{N-2} a_t(N) = \frac{N^2(N-1)^2}{4}. \quad (41)$$

We see that (40) takes into account long-range correlations. In fact, $(\bar{\xi}^2)_t \rightarrow \bar{\xi}^2$, and $a_t(N)$ decreases for $t \geq 3$. It allows us to reduce (38) according to the random walk ideology.

It seems natural to introduce $\|\xi_{i,j}\|$ as

$$\xi_{i,j} = \sum_{g \in G} \rho_g(i,j) [\text{dist}_{\mathbb{B}}(\mathbf{0}, g\gamma_j\gamma_i[\mathbf{0}]) - \text{dist}_{\mathbb{B}}(\mathbf{0}, g\gamma_j[\mathbf{0}])], \quad (42)$$

where $G \subset \Gamma_{\text{BRC}}$ is a some (finite) set of generators g ; ρ_g is the weight for each g .

Note that (42) generalizes the expression from [28], where $g = \text{id}$ is used in a two-dimensional model. Here, the reason for involving additional g is to obtain sufficiently large values of the hyperbolic distance when $\cosh, \sinh \rightarrow 1/2 \exp$ in (31).

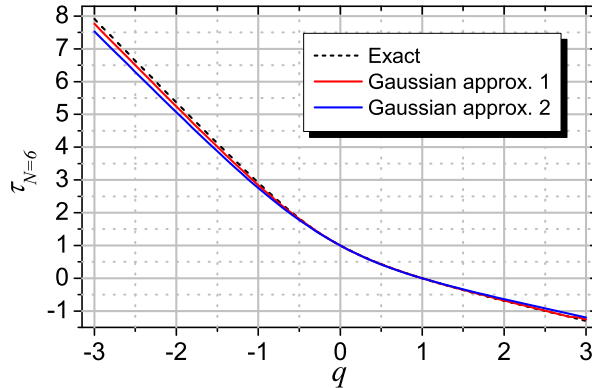


Figure 6: Scaling exponent $\tau_N(q)$ for $N = 6$ and its approximations. Both approximations (colored lines) are based on the Gaussian form (30) for different sets of parameters: the red line uses the exact characteristics \mathcal{L}_{\min} , \mathcal{L}_{\max} , $\bar{\mathcal{L}}_N$, and σ_N , while the blue line uses the parameters (37), (38) in the Markov approximation.

Here we test the implementation, when G is just the generating set (16):

$$\xi_{i,j} = \frac{1}{5} \sum_{k=1}^6 p_2(j,k) [\text{dist}_{\mathbb{B}}(\mathbf{0}, \gamma_k\gamma_j\gamma_i[\mathbf{0}]) - \text{dist}_{\mathbb{B}}(\mathbf{0}, \gamma_k\gamma_j[\mathbf{0}])]. \quad (43)$$

Applying this definition for $N = 6$ gives us $\mathcal{L}_{\min}^*(N) \simeq 12.8784$, $\mathcal{L}_{\max}^*(N) \simeq 33.1276$, $\bar{\mathcal{L}}_N^* \simeq 24.6803$, and $\sigma_N^* \simeq 2.85126$, while the exact parameters are $\mathcal{L}_{\min}(N) \simeq 13.0367$, $\mathcal{L}_{\max}(N) \simeq 33.0990$, $\bar{\mathcal{L}}_N \simeq 25.0977$, and $\sigma_N \simeq 3.13207$. By substituting these two sets into (30) and calculating $\tau_N(q)$ using (24), we are able to compare the approximations for relatively small $|q|$ in Fig. 6. Physically, the situation corresponds to the high-temperature mean-field approximation, since $q \sim 1/T$. Although the double approximation worsens the description, it eliminates the need to calculate the \mathcal{L} 's spectrum. We leave possible improvements for further research. Some aspects regarding the ergodicity of the model may also be clarified.

4 Deformations and Teichmüller space

Let us determine the deformation space $\text{Def}(M)$ for orbifold $M \simeq \mathbb{B}/\Gamma_{\text{BRC}}$ by using the Mostow's generalized rigidity theorem [1]. Then the deformation space of hyperbolic three-manifold M may be defined as

$$\text{Def}(M) \simeq \text{Teich}(\partial M), \quad (44)$$

where $\text{Teich}(\partial M)$ is the Teichmüller space of the marked structures on the closed and oriented surface ∂M .

A crucial step towards our goal is the description of the Teichmüller space $\text{Teich}(\Sigma)$ associated with the octahedral surface Σ having six cusps and $S_4 \times \mathbb{Z}_2$ symmetry, as shown in Fig. 2(right). Marking Σ and stabilizing each of the ideal vertices of Σ with the Abelian subgroup $A_i = \langle \gamma_i, \tilde{\gamma}_i \in \Gamma_{\text{BRC}} | \gamma_i^n \tilde{\gamma}_i^m = \tilde{\gamma}_i^m \gamma_i^n \rangle$ formed by the meridian and longitude for $i = \bar{1}, \bar{6}$, we first build the decorated Teichmüller space $\mathcal{T}(\Sigma)$ [5], that is, the space of hyperbolic cusp metrics on Σ with the addition of horospheres centered at the cusps. Removing decoration implies projection $\mathcal{T}(\Sigma) \mapsto \text{Teich}(\Sigma)$.

Using the radius-vectors $\mathbf{e}_{\pm x} = (\pm 1 \ 0 \ 0)^\top$, $\mathbf{e}_{\pm y} = (0 \ \pm 1 \ 0)^\top$, and $\mathbf{e}_{\pm t} = (0 \ 0 \ \pm 1)^\top$ for the cusps, let us define the vertex set $V = \{\mathbf{e}_{\pm x}, \mathbf{e}_{\pm y}, \mathbf{e}_{\pm t}\}$ with the cardinality $|V| = 6$, and the geodesic edge set $E = \{E_{ji}\}$ with $|E| = 12$, appropriately connecting the vertices $\mathbf{e}_j, \mathbf{e}_i \in V$ of the octahedron. Hereafter, we denote the triangular faces as F_i (or Δ_i) with evident $|F| = 8$.

Decorating the octahedron by means of the set of horospheres $H = \{H_{\pm x}, H_{\pm y}, H_{\pm t}\}$ centered at the cusps V , all discrete metrics (finite lengths of edge segments bounded by H) form a manifold of real dimension $|E|$. This manifold is fibered by the discrete conformal classes representing submanifolds of dimension $|V|$. Besides, conformal equivalence of the metric sets also admits conformality of triangulations of the octahedron faces. Thus, the discrete conformal class correspond to a point in the Teichmüller space $\mathcal{T}_{|V|}$ endowed with the mapping class group $\pi_0(\text{Aut}(\Sigma))$, which is isomorphic to the braid group of vertex permutations.

4.1 Decorating the octahedral surface

We start to describe the decorated geometry in terms of the set of Euclidean heights² $h = \{h_{\pm x}, h_{\pm y}, h_{\pm t}\}$, $h_i \in [0; 1]$, determining the location of the horospheres H so that $h_i \mathbf{e}_i$ is the point of H_i closest to the origin (see Fig. 7). We obtain that the endpoint of the E_{ji} -edge segment terminating at H_i is specified by the radius-vector:

$$\mathbf{e}_{j,i} = 2 \frac{(1 - h_i)^2}{(1 - h_i)^2 + 4} \mathbf{e}_j + \frac{(1 + h_i)^2}{(1 - h_i)^2 + 4} \mathbf{e}_i, \quad (45)$$

²We hope that the same notation h_i for generators in Sec. 2 and for heights here will not cause confusion due to the context.

which tends to $\mathbf{e}_i \in \partial\mathbb{B}$ when $h_i \rightarrow 1$. The other end of the same edge segment is given by $\mathbf{e}_{i,j}$. Then, for two adjacent vertices i, j and the corresponding heights h_i, h_j we have that the signed hyperbolic length between $\mathbf{e}_{j,i}$ and $\mathbf{e}_{i,j}$ is

$$\rho(h_i, h_j) = 2 \operatorname{arcsinh} \frac{3(h_i + h_j) - h_i h_j - 1}{2\sqrt{2(1-h_i^2)(1-h_j^2)}}. \quad (46)$$

Note that if the horospheres overlap, $\rho(h_i, h_j)$ becomes negative.

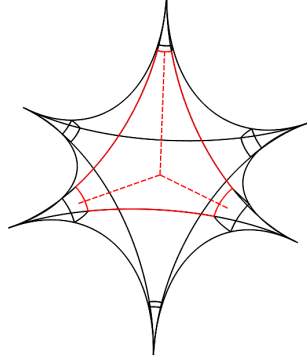


Figure 7: Decorated octahedral surface. Intersecting the octahedral surface, each horosphere H_i , centered at octahedron ideal vertex \mathbf{e}_i , produces a square with right angles. Arbitrarily choosing the heights h_i , that is, the Euclidean distances from the horospheres to the origin (red dashed lines), we obtain on each octahedron face a hexagon similar to the one formed from the red curves. The lengths of the red segments of the octahedron edges are equal to $\lambda_{i,j}$, while the length of each edge of the square contour around the cuspidal tail is determined by w_i .

Thus, $\lambda_{i,j} = \rho(h_i, h_j)$ produce the set $\Lambda = \{\lambda_{\pm x, \pm y}, \lambda_{\pm x, \pm t}, \lambda_{\pm y, \pm t}\} \in \mathbb{R}^{|E|}$ of λ -lengths (need not be distinct) of the decorated octahedron edges. These Λ s serve as coordinates of Teichmüller space. However, the number of independent parameters remains equal to $|V|$, and they can be further considered as moduli.

Note that the vector tangent to the edge $E_{j,i}$ at the endpoint $\mathbf{e}_{j,i}$ is

$$\mathbf{v}_{j,i} = (3 - h_i)(1 + h_i)\mathbf{e}_i - 4(1 - h_i)\mathbf{e}_j. \quad (47)$$

We also need the lengths w_i of non-empty paths $F_j \cap H_i$ connecting the nearby ends $\mathbf{e}_{j\alpha,i}$ of the reduced edges $E_{j\alpha,i}$. It is expected that $w_i \geq \operatorname{dist}_{\mathbb{B}}(\mathbf{e}_{j_1,i}, \mathbf{e}_{j_2,i})$, where the ends $\mathbf{e}_{j_1,i}, \mathbf{e}_{j_2,i} \in F_j \cap H_i$, and $w_i \rightarrow 0$ at $h_i \rightarrow 1$.

Thus, the length $w_i = w(h_i)$ can be obtained by directly integrating $d\mathbb{S}_{\mathbb{B}}$ along the parametrized path between the nearby ends belonging to H_i and is given by

$$w(h) = \sqrt{2} \frac{1-h}{1+h}, \quad (48)$$

see Appendix B for details.

Therefore, decoration actually results in applying a right-angled hexagon to each face F_i of the octahedron (see Fig. 7), using two sets of lengths: $\{\lambda_{i_2,i_1}, \lambda_{i_3,i_1}, \lambda_{i_2,i_3}\}$ and $\{w_{i_1}, w_{i_2}, w_{i_3}\}$. Since the right angles of hexagons are preserved for an arbitrary height set h , the decoration has conformal property. As argued in [15, 16, 31], we may additionally complicate the structure by triangulating the hexagons.

Indeed, function $w(h)$ is the subject of the identity:

$$w(h) = w(\tilde{h}) e^{\epsilon\tau_e}, \quad \tau_e = \operatorname{dist}_{\mathbb{B}}(h\mathbf{e}, \tilde{h}\mathbf{e}), \quad \epsilon = \operatorname{sign}(\tilde{h} - h), \quad \mathbf{e} \in V. \quad (49)$$

This relation induces the boost of the height h for vertex \mathbf{e} :

$$\tilde{h} = \frac{h + \tanh(u_{\mathbf{e}}/2)}{1 + h \tanh(u_{\mathbf{e}}/2)}, \quad (50)$$

where $u_{\mathbf{e}} \in \mathbb{R}$ and should be equal to $\epsilon\tau_{\mathbf{e}}$ to reproduce (49).

Additional relations appear when introducing the midpoint of the edge E_{ji} , i.e. $\mathbf{m}_{j,i} = (1 - 2^{-1/2})(\mathbf{e}_j + \mathbf{e}_i)$, and the distances determined by h_i and h_j :

$$p_{j,i} = \text{dist}_{\mathbb{B}}(\mathbf{m}_{j,i}, \mathbf{e}_{j,i}), \quad p_{i,j} = \text{dist}_{\mathbb{B}}(\mathbf{m}_{j,i}, \mathbf{e}_{i,j}), \quad (51)$$

so that $\lambda_{j,i} = p_{j,i} + p_{i,j}$. We have that $w_i = \exp(-p_{j,i})$ and $w_j = \exp(-p_{i,j})$ [5].

For ideal triangle Δ_i (octahedron face F_i) with vertices $\{\mathbf{e}_{i_1}, \mathbf{e}_{i_2}, \mathbf{e}_{i_3}\}$ decorated by horospheres $\{H_{i_1}, H_{i_2}, H_{i_3}\}$, we are focusing on the configurations corresponding to the triangle inequalities:

$$\lambda_{i_2, i_1} + \lambda_{i_3, i_1} > \lambda_{i_2, i_3}, \quad \lambda_{i_2, i_1} + \lambda_{i_2, i_3} > \lambda_{i_3, i_1}, \quad \lambda_{i_3, i_1} + \lambda_{i_2, i_3} > \lambda_{i_2, i_1}. \quad (52)$$

Denoting $p_{i_2, i_1} = p_{i_3, i_1} \equiv a_i$, $p_{i_1, i_2} = p_{i_3, i_2} \equiv b_i$, and $p_{i_2, i_3} = p_{i_1, i_3} \equiv c_i$, one has $\lambda_{i_2, i_1} = a_i + b_i$, $\lambda_{i_3, i_1} = a_i + c_i$, and $\lambda_{i_2, i_3} = b_i + c_i$. We see that [15]

$$\begin{aligned} w_{i_1} &= e^{-a_i}, & a_i &= \frac{1}{2}(\lambda_{i_2, i_1} + \lambda_{i_3, i_1} - \lambda_{i_2, i_3}), \\ w_{i_2} &= e^{-b_i}, & b_i &= \frac{1}{2}(\lambda_{i_2, i_1} + \lambda_{i_2, i_3} - \lambda_{i_3, i_1}), \\ w_{i_3} &= e^{-c_i}, & c_i &= \frac{1}{2}(\lambda_{i_3, i_1} + \lambda_{i_2, i_3} - \lambda_{i_2, i_1}). \end{aligned} \quad (53)$$

Conversely, we claim that $\lambda_{i,j} = -\ln(w_i w_j)$.

Parameterizing $h_i = \tanh(u_i/2)$ by $\bar{u}_i = u_i - \frac{1}{2} \ln 2$ for $i = \overline{1, |V|}$, the discrete conformal metrics are determined as

$$w_i = e^{-\bar{u}_i}, \quad \ell_{i,j} = e^{\lambda_{i,j}/2}, \quad \lambda_{i,j} = \bar{u}_i + \bar{u}_j, \quad (54)$$

where $\ell_{i,j}$ and w_i are the Penner's lengths and heights [5]. Then, two extended sets $\{\lambda_{i,j}^{(1)}, w_i^{(1)}\}$ and $\{\lambda_{i,j}^{(2)}, w_i^{(2)}\}$ belong to the same discrete conformal class and are *isometric* if there exists a one-parameter Möbius transformation:

$$h_i^{(2)} = \frac{h_i^{(1)} + \tanh(\tau/2)}{1 + h_i^{(1)} \tanh(\tau/2)}, \quad \bar{u}_i^{(2)} = \bar{u}_i^{(1)} + \tau, \quad i = \overline{1, |V|}. \quad (55)$$

Thus, an ordered tuple $U_0 = \{\bar{u}_{\pm x}, \bar{u}_{\pm y}, \bar{u}_{\pm t}\}$ of six fixed positive numbers produces the equivalence class $\{U_\tau\}$ preserving a marking, where each set $U_\tau = \{\bar{u}_{\pm x} + \tau, \bar{u}_{\pm y} + \tau, \bar{u}_{\pm t} + \tau\}$ has non-negative components for $\tau \in \mathbb{R}$.

Conformal stretching of the surface structure can be generated by a convex "energy" function $\mathcal{E}(\{\bar{u}_i\})$ so that

$$\frac{d\bar{u}_i}{d\tau} = -\frac{\partial \mathcal{E}(\{\bar{u}_i\})}{\partial \bar{u}_i}. \quad (56)$$

This equation is similar to the discrete Ricci/Yamabe flow [15, 16], and the volume of cuspidal tails truncated by horospheres can serve as $\mathcal{E}(\{\bar{u}_i\})$. As an alternative, other functions are also proposed in [15, 16].

4.2 The mapping class group

Some permutations of \bar{u}_i in U_0 , which lead to an inequivalent \tilde{U} , could preserve the face hexagons constructed on the base of U_0 . They are generated by two fourth-order rotations about the orthogonal axis, which determine the *mapping class group* $\mathcal{G}^* = \langle \hat{\tau}_1, \hat{\tau}_2 \mid \hat{\tau}_1^4 = \hat{\tau}_2^4 = 1 \rangle$ [32]. Representatives of \mathcal{G}^* rearrange the vertices of the cyclic boundaries defined as follows.

Let $\{\Delta_\alpha \mid \alpha = \overline{1,4}\}$ be a cycle of adjacent triangles (octahedron faces) so that $\Delta_\alpha \cap \Delta_{\alpha+1} = E_\alpha$, where we regard the index α as cyclic, $\Delta_5 = \Delta_1$. Denoting the ideal edges of Δ_α as $\{E_{\alpha-1}, E_\alpha, \tilde{E}_\alpha\}$, the collection $\{\tilde{E}_\alpha \mid \alpha = \overline{1,4}\}$ forms boundary of the cycle $\{\Delta_\alpha \mid \alpha = \overline{1,4}\}$. Obviously, in the planes $\mathbb{D}_{t=0}$, $\mathbb{D}_{y=0}$, $\mathbb{D}_{x=0}$ there are three four-sided boundaries separating three pairs of triangle cycles.

Operating by $\hat{\tau}_k$, four heights \bar{u}_i are cyclically permuted in one of such planes, while the rest two heights lying on the axis orthogonal to the plane are fixed. Thereby we determine the *Dehn twists* in three orthogonal planes:

$$\begin{aligned} \hat{\tau}_1[U_0] &= \{\bar{u}_{\mp y}, \bar{u}_{\pm x}, \bar{u}_{\pm t}\}, & \hat{\tau}_1^{-1}[U_0] &= \{\bar{u}_{\pm y}, \bar{u}_{\mp x}, \bar{u}_{\pm t}\}, \\ \hat{\tau}_2[U_0] &= \{\bar{u}_{\mp t}, \bar{u}_{\pm y}, \bar{u}_{\pm x}\}, & \hat{\tau}_2^{-1}[U_0] &= \{\bar{u}_{\pm t}, \bar{u}_{\mp y}, \bar{u}_{\mp x}\}, \\ \hat{\tau}_3[U_0] &= \{\bar{u}_{\pm x}, \bar{u}_{\mp t}, \bar{u}_{\pm y}\}, & \hat{\tau}_3^{-1}[U_0] &= \{\bar{u}_{\pm x}, \bar{u}_{\pm t}, \bar{u}_{\mp y}\}, \end{aligned} \quad (57)$$

where $\hat{\tau}_3 = \hat{\tau}_1^{-1} \hat{\tau}_2^{-1} \hat{\tau}_1$, and $\hat{\tau}_1 \hat{\tau}_2 \hat{\tau}_1 = \hat{\tau}_2 \hat{\tau}_1 \hat{\tau}_2$ from the braid group B_3 .

It means that any two different markings of the octahedral surface are related by the action of the mapping class group \mathcal{G}^* . We immediately deduce that the *moduli space* is $\mathcal{M}^*(\Sigma) \simeq \mathbb{R}_+^{|V|} / \mathcal{G}^*$.

Note that the mapping class group, acting combinatorially on six (unmarked) punctures of the sphere $\partial\mathbb{B}$, is associated to the braid group B_6 [33]. This could be also considered as the starting point of our reasoning [32].

To formalize the action of \mathcal{G}^* , we introduce the six-dimensional vector

$$\mathbf{u} = \begin{pmatrix} 1 \\ 0 \end{pmatrix} \otimes \mathbf{u}_+ + \begin{pmatrix} 0 \\ 1 \end{pmatrix} \otimes \mathbf{u}_-, \quad \mathbf{u}_\pm = \begin{pmatrix} \bar{u}_{\pm x} \\ \bar{u}_{\pm y} \\ \bar{u}_{\pm t} \end{pmatrix}. \quad (58)$$

Thus, the implementation $\rho : \mathcal{G}^* \mapsto \text{Mat}(6, \{0, 1\})$ is given by the matrices of permutations $T_i = \rho(\hat{\tau}_i)$, expanded due to the Kronecker multiplication as

$$T_i = I_2 \otimes M_i + J_2 \otimes N_i, \quad (59)$$

$$I_2 = \begin{pmatrix} 1 & 0 \\ 0 & 1 \end{pmatrix}, \quad J_2 = \begin{pmatrix} 0 & 1 \\ 1 & 0 \end{pmatrix}, \quad (60)$$

$$M_1 = \begin{pmatrix} 0 & 0 & 0 \\ 1 & 0 & 0 \\ 0 & 0 & 1 \end{pmatrix}, \quad M_2 = \begin{pmatrix} 0 & 0 & 0 \\ 0 & 1 & 0 \\ 1 & 0 & 0 \end{pmatrix}, \quad M_3 = \begin{pmatrix} 1 & 0 & 0 \\ 0 & 0 & 0 \\ 0 & 1 & 0 \end{pmatrix}, \quad (61)$$

$$N_1 = \begin{pmatrix} 0 & 1 & 0 \\ 0 & 0 & 0 \\ 0 & 0 & 0 \end{pmatrix}, \quad N_2 = \begin{pmatrix} 0 & 0 & 1 \\ 0 & 0 & 0 \\ 0 & 0 & 0 \end{pmatrix}, \quad N_3 = \begin{pmatrix} 0 & 0 & 0 \\ 0 & 0 & 1 \\ 0 & 0 & 0 \end{pmatrix}, \quad (62)$$

so that $T_i^4 = I_6$ and $\det T_i = -1$; I_n is the unit matrix in n dimensions.

One has $\rho(g_1 g_2) = \rho(g_1) \rho(g_2)$ for $g_{1,2} \in \mathcal{G}^*$, and

$$T_i^{-1} = I_2 \otimes M_i^\top + J_2 \otimes N_i^\top, \quad (63)$$

$$T_i T_j = I_2 \otimes (M_i M_j + N_i N_j) + J_2 \otimes (M_i N_j + N_i M_j), \quad (64)$$

$$T_i \mathbf{u} = \begin{pmatrix} 1 \\ 0 \end{pmatrix} \otimes (M_i \mathbf{u}_+ + N_i \mathbf{u}_-) + \begin{pmatrix} 0 \\ 1 \end{pmatrix} \otimes (M_i \mathbf{u}_- + N_i \mathbf{u}_+), \quad (65)$$

where $J_2^2 = I_2$ and $N_i N_j = 0$ by construction.

The new configuration is then determined by $\tilde{\mathbf{u}} = \rho(g)[\mathbf{u}]$, $g \in \mathcal{G}^*$. Obviously, the permutations preserve the form:

$$\xi_n = \sum_{s=x,y,t} (\bar{u}_{+s}^n + \bar{u}_{-s}^n), \quad n \in \mathbb{N}. \quad (66)$$

Setting $J = T_1 T_2$ and $S = T_1 J$ results in the relation $S^2 = J^3 = I_6$ inherent in $PSL(2, \mathbb{Z}) \simeq \mathbb{Z}_2 * \mathbb{Z}_3$, and B_3 looks like the central extension of $PSL(2, \mathbb{Z})$ [34]. We also note the q -deformed analogue of B_3 , presented and discussed in [35].

To describe the group structure, we represent T_i , $i = \overline{1, 3}$, in the form:

$$T_i = I_2 \otimes R_i + (I_2 + J_2) \otimes N_i, \quad R_i = M_i - N_i. \quad (67)$$

We find that each $R_i = \exp(\frac{\pi}{2} X_i)$ is generated by X_i from $so(3)$ algebra:

$$X_1 = \begin{pmatrix} 0 & -1 & 0 \\ 1 & 0 & 0 \\ 0 & 0 & 0 \end{pmatrix}, \quad X_2 = \begin{pmatrix} 0 & 0 & -1 \\ 0 & 0 & 0 \\ 1 & 0 & 0 \end{pmatrix}, \quad X_3 = \begin{pmatrix} 0 & 0 & 0 \\ 0 & 0 & -1 \\ 0 & 1 & 0 \end{pmatrix}, \quad (68)$$

$$[X_i, X_j] = \varepsilon_{ijk} X_k, \quad \{i, j, k\} = \{1, 2, 3\}, \quad (69)$$

where ε_{ijk} is the Levi-Civita tensor, and the Casimir operator is then equal to

$$X_1^2 + X_2^2 + X_3^2 = -2I_3. \quad (70)$$

Further, introducing $\mathcal{R}_i = I_2 \otimes R_i = \exp(\frac{\pi}{2} I_2 \otimes X_i)$, we decompose T_i as

$$T_i = \mathcal{R}_i \mathcal{A}_i, \quad \mathcal{A}_i = I_2 \otimes (I_3 + R_i^{-1} N_i) + J_2 \otimes (R_i^{-1} N_i), \quad (71)$$

where $\mathcal{A}_i^2 = I_6$ indicates the second-order cyclic relation.

Excluding $\langle \mathcal{A}_1, \mathcal{A}_2 \rangle$ from \mathcal{G}^* , we are left with the group $\langle R_1, R_2 | R_1^4 = R_2^4 = I_3 \rangle$ in $SO(3)$, which permutes α_s in initial vector $\boldsymbol{\alpha} = (\alpha_x \ \alpha_y \ \alpha_t)^\top \in \mathbb{R}^3$, when identifying

$$\alpha_s \leftrightarrow \bar{u}_{\pm s}, \quad -\alpha_s \leftrightarrow \bar{u}_{\mp s}, \quad s = \{x, y, t\}. \quad (72)$$

This completes the analysis of the structure of the mapping class group \mathcal{G}^* operating in Euclidean (moduli) space [33] and leaving the following interval invariant:

$$ds_{\mathcal{M}}^2 = \sum_{s=x,y,t} (d\bar{u}_{+s}^2 + d\bar{u}_{-s}^2). \quad (73)$$

On the other hand, assigning positive real numbers to the octahedron ideal edges ($E_{ij} \mapsto \lambda_{i,j}$) and thereby defining the point $P \in \mathcal{T}(\Sigma)$ in Teichmüller space, then λ -lengths are natural for the action of the mapping class group $\mathcal{G}(\Sigma)$. Thus, $\mathcal{G}(\Sigma)$ acts on $\mathcal{T}(\Sigma)$. If $\varphi \in \mathcal{G}(\Sigma)$, there is a map $\varphi_* : \mathcal{T}(\Sigma) \mapsto \mathcal{T}(\Sigma)$, which for an arc E gives $\lambda(E; P) = \lambda(\varphi E; \varphi_* P)$. Since the point T is determined by Λ -set, it is easy to show that $\varphi_* = \varphi^{-1}$. Having already described the action of the mapping class group \mathcal{G}^* , we omit here explicit transformations of λ -lengths, which become identities using U and $g[U]$, where $g \in \mathcal{G}^*$.

Thus, when formulating physical models, it is possible to take into account the conformality of surface structures and their transformations under the action of mapping class group. One of the attractive aspects of further study is the geometry quantization.

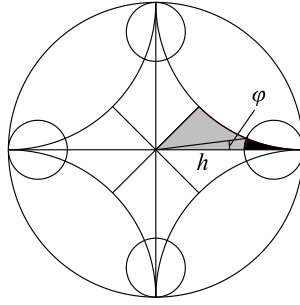


Figure 8: Decorated ideal square divided into eight parts. The gray segment area A_Δ is given by Eq. (74), where the defect $\pi/4 - A_\Delta$ determines the area of black cuspidal tail.

4.3 Towards area quantization

Consider a star-shaped body bounded by the octahedron edges and formed by three ideal squares lying in orthogonal planes $\mathbb{D}_{t=0}$, $\mathbb{D}_{y=0}$, $\mathbb{D}_{x=0}$. Let us analyze how to approach a quantum spectrum of the area of such squares.

Dissecting the one decorated square into eight parts (see Fig. 8), we obtain that the area of each part depends on the height h as

$$A_\Delta(h) = \frac{\pi}{4} - \frac{1-h}{1+h}. \quad (74)$$

For simplicity, we set $h_i = h \in [2^{-1/2}; 1]$ for $i = \{\pm x, \pm y, \pm t\}$ and write down the total area of the right-angled octagon as $A = 8A_\Delta$.

Regarding $h = \tanh(u/2)$ as above, we obtain the geometric relations:

$$\frac{1-h}{1+h} = e^{-u} = \sqrt{\frac{1}{2} \tan \varphi}, \quad (75)$$

where the angle φ is indicated in Fig. 8. Note that (75) is exactly equal to the hyperbolic length of horocircle segment being the fourth edge of the gray region.

This immediately leads to the (stationary) antikink:

$$\varphi(\bar{u}) = \arctan e^{-2\bar{u}}, \quad \bar{u} \in [0; +\infty), \quad (76)$$

where the module $\bar{u} = u - \frac{1}{2} \ln 2$ is such that introduced earlier.

Thus, (76) is a subject of a one-dimensional sine-Gordon model with the following action integral and equation of motion [17]:

$$S = \int \left\{ \frac{1}{2} (\partial_{\bar{u}} \varphi)^2 + \frac{1}{4} [1 - \cos(4\varphi)] \right\} d\bar{u}, \quad (77)$$

$$\partial_{\bar{u}}^2 \varphi - \sin(4\varphi) = 0, \quad (78)$$

which are invariant under the global transformation $\varphi \rightarrow \varphi + \pi n/2$, $n \in \mathbb{N}$. In the general case of distinct heights h_i , S is being evidently written for a sextet of fields $\{\varphi_i | i = 1, |\bar{V}|, |V| = 6\}$, preserving invariance under the permutations induced by the mapping class group. In the absence of interaction between the sextet components, the equations of motion take the form (78), but differ in the initial conditions.

The energy of (76) is determined by the integral:

$$\int_0^\infty \left\{ (\partial_{\bar{u}} \varphi)^2 + \frac{1}{2} [1 - \cos(4\varphi)] \right\} d\bar{u} = 1. \quad (79)$$

We assume that our problem concerns the quantization of the relation:

$$2 \left(\frac{\pi}{4} - A_\Delta \right)^2 = \tan \varphi, \quad (80)$$

where the right-hand side reduces to the form in term of the self-action W :

$$\tan \varphi = \frac{\sqrt{W(\varphi)}}{1 + \sqrt{1 - W(\varphi)}}, \quad W(\varphi) = \frac{1}{2} [1 - \cos(4\varphi)]. \quad (81)$$

We leave the search for a solution and exploration to future work that needs to show possible connection with low-dimensional loop quantum gravity and spin foam [11, 36]. A similar task would arise when quantizing lengths (see also [18]).

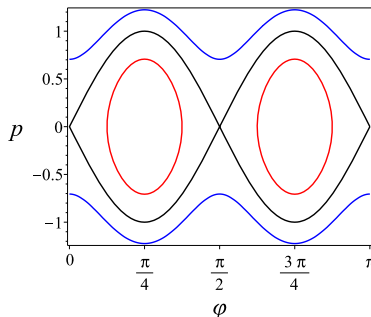


Figure 9: Phase portrait of trajectories at fixed energy H in (82). The black curve corresponds to $H = 0$. Blue curve is typical for $H > 0$ (the scattering), while the red curve is for $H < 0$. At $H = -1/2$, the ellipses are contracted into points with the coordinates $((2n + 1)\pi/4; 0)$, $n \in \mathbb{Z}$.

Finally, we would like to analyze the area of phase space. Introducing the canonical momentum $p = \partial_{\dot{a}}\varphi$, inducing the Poisson bracket $\{\varphi, p\} = 1$, and taking into account that $W(\varphi) = \sin^2(2\varphi)$, the dynamics is generated by the Hamiltonian:

$$H = \frac{p^2 - \sin^2(2\varphi)}{2}. \quad (82)$$

The regimes of such a model are depicted in Fig. 9.

The solution (76) corresponds to $H = 0$ and serves as a boundary for the mode $H < 0$ with cyclic trajectories. Denoting $\varepsilon = -2H \geq 0$ in these cases, let us define the action variable associated with the “quantum” of phase-space area:

$$J \equiv \oint p(\varphi) d\varphi = -4 \int_{\varphi_0(\varepsilon)}^{\pi/4} \sqrt{W(\varphi) - \varepsilon} d\varphi \quad (83)$$

$$= 2E(\sqrt{1 - \varepsilon}) - 2\varepsilon K(\sqrt{1 - \varepsilon}), \quad (84)$$

where $\varphi_0(\varepsilon) = (1/2)\arcsin\sqrt{\varepsilon}$; $K(k)$ and $E(k)$ are the complete elliptic integrals of the first and second kind, respectively [30]. Hence, the area of $n \in \mathbb{N}$ (red or black) cycles at $\varepsilon \in [0; 1)$ is equal to $nJ(\varepsilon)$, where $J(0) = 2$ and $J(1) = 0$.

Of course, the obtained results are easily generalized for the case of distinct heights h_i , when the induced symplectic 2-form becomes $\omega = \sum_{i=1,6} dp_i \wedge d\varphi_i$. This is seen as a tool for constructing an algebra whose generator spectra solve the quantization problem [19, 20].

5 Discussion

Embedding all the structures associated with the Borromean rings complement (BRC) into the Poincaré unit ball \mathbb{B} with its isometry group $\text{Isom}(\mathbb{B})$, we begin with a description of the BRC geometry and finding the realization $\Gamma_{\text{BRC}} \subset \text{Isom}(\mathbb{B})$ of the fundamental group $\pi_1(\text{BRC}) \simeq \mathbb{Z}_2^3 \rtimes \mathcal{C}_3$. Using Thurston's proposal regarding the BRC tessellation of two octahedra [1], we do this in several steps.

We found it convenient to first fix the four-vertex basis of one octahedron in the plane of unit disc \mathbb{D} by using the parabolic $SU(1, 1)$ -isometries (see Fig. 2). Having extended the action of the parabolic generators up to three dimensions due to transformation from [3] and further operating with rotations around the main axes, we obtain the overfull set of twelve generators. Namely, we arrive at six pairs of parabolic generators $\langle h_i, \tilde{h}_i \rangle$ of longitudes and meridians, which fix each of the six vertices of the octahedron and form Abelian subgroups (see Appendix A).

Next, we choose three pairs of generators (14) related to distinct axes. They correspond to the torus T^3 and are isomorphic to the BRC fundamental group [4]. To obtain Γ_{BRC} in the Wirtinger representation (13), we express three of the six generators in terms of the remaining ones (15), chosen as independent.

Thus, we first get twelve generators operating in three dimensions, and then reduce their number to six and finally to three. This allows us to analyze the structure of Γ_{BRC} and to apply it in geometry and constructing Teichmüller space. Indeed, twelve non-independent generators are convenient for tiling \mathbb{B} with octahedra, as well as for obtaining the maximally symmetric complement [25] represented by the rhombic dodecahedron in Fig. 3(right). Perhaps the applied scheme will also be useful for implementing the group in terms of quaternions [24].

Having realized the group Γ_{BRC} , it is natural to turn to the problem of obtaining functions that are invariant under the action of the group. In fact, it was constructed in [3] a functional basis consisting of Jacobi θ -functions symmetrized with respect to the BRC group as a subgroup of $SL(2, \mathbb{C})$.

Here, we consider the Cayley tree rooted at the origin and embedded in the ball \mathbb{B} for the group Γ_{BRC} and focus on the multifractal properties of the partition function $\mathcal{Z}_N(q)$ from (20) defined for a truncated tree up to N th generation. It is viewed as a kind of Poincaré series of the Boltzmann weights for discrete paths, where the moment order q corresponds to the inverse temperature $1/T$ in physics and takes positive and negative values. Since the conventional Poincaré series of Boltzmann weights, determined by the only hyperbolic distance of order N , between the vertices of the tree, does not exhibit multifractality, we use the functional \mathcal{L} with an ‘‘interaction’’ of the form (21) and order N^2 . This is similar to the perimetric characteristic of the surface formed by adjacent triangles connecting the root point and two nearby vertices [28]. Besides, the six-branch graphs that emerged there can imitate dendritic polymers [13].

Numerical analysis revealed fast stochastization of \mathcal{L} with increasing N and multifractal behavior of $\mathcal{Z}_N(q)$ (see Fig. 4), when the exponents of its characteristics are simply compared for different models and admit a physical interpretation [14].

Thus, the obtained multifractal exponents, such as the fractal dimensions, indicate the absence of a dominant subset of paths and the need to take into account all graphs, at least approximately, in the desired analytical description. On the other hand, for large N the behavior becomes conditioned by the central limit theorem. This allowed us to apply Markov chains (random walk) and calculate the partition function in the Gaussian approximation (mean field approximation in physics), valid for relatively small $|q|$ (see Fig. 6). Note that for a better analytical description it was necessary to improve the formula for transition matrix (43), the introduction of which eliminates the need to numerically calculate the \mathcal{L} -spectrum for all graphs.

Touching upon the concept of the deformation space in the last part of our work, we appeal to the generalized Mostow's theorem [1]. Thus, the key point to describing the deformations of the quotient $\mathbb{B}/\Gamma_{\text{BRC}}$ is the decorated Teichmüller space of conformal structures on the regular octahedral surface with ideal vertices (cusps). Here we follow Penner's receipt [5], although there is its generalization in [37].

Decorating the octahedral surface involves incorporating horospheres with the centers at the vertices and obtaining curves of their intersection with octahedron faces, which always remain orthogonal to the octahedron edges. Conformality is justified by maintaining right angles regardless of the size of each horosphere, which is regulated by boost [5, 15, 16].

According to Penner [5], the decorated Teichmüller space, when a surface *is marked* by a particular realization of the fundamental group, consists of sets of finite hyperbolic lengths of edge segments bounded by horospheres. It is due to the fact that the octahedron faces are ideal triangles, i.e. the octahedral surface is initially triangulated. And we may introduce the manifold $\mathbb{R}_+^{|E|}$ for the number of edges $|E| = 12$.

However, by fibering, information is encoded in $\mathcal{T}_{|V|} \simeq \mathbb{R}_+^{|V|}$ at $|V| = 6$ that is the number of vertices. Geometrically, this means that the set of six positive real numbers (heights), which are the distances from the origin to the horospheres in the direction of the vertices, defines all the elements of the global structure (see Fig. 7). Two such sets are isometrically equivalent and belong to the same *equivalence class* if they are related by a one-parameter Möbius transform (boost). Besides, the ordered set of six hyperbolic lengths is the object of the action of the mapping class group \mathcal{G}^* .

To maintain the conformal structure induced by the decoration on the octahedral surface, the group \mathcal{G}^* acts on the ordered set by cyclic permutations, which are generated by two fourth-order rotations [32]. We are implementing \mathcal{G}^* in Sec. 4.2, describing its structure, and reducing it to a subgroup of $SO(3)$. On the other hand, \mathcal{G}^* can be considered as a permutation group of punctures on $\partial\mathbb{B}$ and associated with the braid group [33]. Anyway, we arrive at the *moduli space* $\mathbb{R}_+^{|V|}/\mathcal{G}^*$ with the Euclidean metric, omitting the operation of the mapping class group in $\mathbb{R}_+^{|E|}$.

With the goal to quantize geometry of the BRC, we were faced with the need to induce a differential two-form and introduce the algebra of observables [18, 19]. In principle, it can be done by means of dynamical model and its symplectic form [20]. Fortunately, by analyzing the area of the decorated square in Fig. 8, we geometrically related the angular size φ of the curve that simultaneously belongs to the horosphere and the face, and the hyperbolic distance \bar{u} from the origin to it. Thereby we arrived at the kink (76) of the one-dimensional sine-Gordon model [17]. Then, passing to the Hamiltonian formalism, the posed problem is resolved in the cotangent bundle. Additionally, using a phase portrait of the model and the action variable, we also took a step towards quantizing the area of the phase space. Although a detailed study of the desired algebra still remains a prospect for the future.

Acknowledgments

A.V.N. thanks to A.M. Gavrilik (BITP) for inspiring discussions and acknowledges support from the National Academy of Sciences of Ukraine (by its project No. 0122U000888) and the Simons Foundation.

A Three-dimensional transformations

Using the extension (10) preserving $ds_{\mathbb{B}}^2$, the generators of Γ induce the group Γ_* of coordinate transformations (parabolic isometries) in three-dimensional ball \mathbb{B} :

$$h_1^n \left[\begin{pmatrix} x \\ y \\ t \end{pmatrix} \right] = \frac{1}{n^2[t^2 + (y-1)^2] + (nx-1)^2} \begin{pmatrix} x - n[x^2 + (y-1)^2 + t^2] \\ y + n^2[x^2 + (y-1)^2 + t^2] - 2nx \\ t \end{pmatrix}, \quad (85)$$

$$h_2^n \left[\begin{pmatrix} x \\ y \\ t \end{pmatrix} \right] = \frac{1}{n^2[t^2 + (x+1)^2] + (ny-1)^2} \begin{pmatrix} x - n^2[(x+1)^2 + y^2 + t^2] + 2ny \\ y - n[(x+1)^2 + y^2 + t^2] \\ t \end{pmatrix}, \quad (86)$$

$$h_3^n \left[\begin{pmatrix} x \\ y \\ t \end{pmatrix} \right] = \frac{1}{n^2[t^2 + (y+1)^2] + (nx+1)^2} \begin{pmatrix} x + n[x^2 + (y+1)^2 + t^2] \\ y - n^2[x^2 + (y+1)^2 + t^2] - 2nx \\ t \end{pmatrix}, \quad (87)$$

$$h_4^n \left[\begin{pmatrix} x \\ y \\ t \end{pmatrix} \right] = \frac{1}{n^2[t^2 + (x-1)^2] + (ny+1)^2} \begin{pmatrix} x + n^2[(x-1)^2 + y^2 + t^2] + 2ny \\ y + n[(x-1)^2 + y^2 + t^2] \\ t \end{pmatrix}. \quad (88)$$

In the plane of \mathbb{D} at $t = 0$, they reduce to linear-fractional transformations $h_k^n[z]$.

To tile \mathbb{B} by octahedra, it needs to extend the group Γ_* by new (parabolic) generators which act in the planes orthogonal to the disc \mathbb{D} :

$$h_+^n \left[\begin{pmatrix} x \\ y \\ t \end{pmatrix} \right] = \frac{1}{n^2[y^2 + (t-1)^2] + (nx+1)^2} \begin{pmatrix} x + n[x^2 + y^2 + (t-1)^2] \\ y \\ t + n^2[x^2 + y^2 + (t-1)^2] + 2nx \end{pmatrix}, \quad (89)$$

$$\tilde{h}_+^n \left[\begin{pmatrix} x \\ y \\ t \end{pmatrix} \right] = \frac{1}{n^2[x^2 + (t-1)^2] + (ny+1)^2} \begin{pmatrix} x \\ y + n[x^2 + y^2 + (t-1)^2] \\ t + n^2[x^2 + y^2 + (t-1)^2] + 2ny \end{pmatrix}, \quad (90)$$

$$h_-^n \left[\begin{pmatrix} x \\ y \\ t \end{pmatrix} \right] = \frac{1}{n^2[y^2 + (t+1)^2] + (nx+1)^2} \begin{pmatrix} x + n[x^2 + y^2 + (t+1)^2] \\ y \\ t - n^2[x^2 + y^2 + (t+1)^2] - 2nx \end{pmatrix}, \quad (91)$$

$$\tilde{h}_-^n \left[\begin{pmatrix} x \\ y \\ t \end{pmatrix} \right] = \frac{1}{n^2[x^2 + (t+1)^2] + (ny+1)^2} \begin{pmatrix} x \\ y + n[x^2 + y^2 + (t+1)^2] \\ t - n^2[x^2 + y^2 + (t+1)^2] - 2ny \end{pmatrix}. \quad (92)$$

Note that h_+ and \tilde{h}_+ (as well as h_- and \tilde{h}_-) refer to the same fixed point. It means that their composition is also a parabolic generator, and $\tilde{h}_\pm^n h_\pm^n = h_\pm^n \tilde{h}_\pm^n$. Looking for \tilde{h}_k , $k = \overline{1,4}$, to create analogous Abelian subgroups, it needs to rotate $h_{1,3}$ by the angle $\pm\pi/2$ around basis vector \mathbf{j} and rotate $h_{2,4}$ around vector \mathbf{i} by using (11). This gives us a pair of generators corresponding to the meridian and longitude at each vertex.

B Calculating $w(h)$

Let us calculate the hyperbolic length $w(h)$ of the red curve C in Fig. 10 resulted from intersection of the octahedral face $(x-1)^2 + (y-1)^2 + (t-1)^2 = 2$ for $0 \leq x, y, t < 1$ and the horosphere $x^2 + y^2 + [t - (1+h)/2]^2 = (1-h)^2/4$ for the cusp $(0 \ 0 \ 1)^\top$. The endpoints of C are

$$\left(0, \frac{2(1-h)^2}{(1-h)^2+4}, \frac{(1+h)^2}{(1-h)^2+4} \right)^\top, \quad \left(\frac{2(1-h)^2}{(1-h)^2+4}, 0, \frac{(1+h)^2}{(1-h)^2+4} \right)^\top. \quad (93)$$

Parametrizing C by $x \in D$ as

$$t(x) = \frac{3 - 2x(1-h) + h^2 - 2\sqrt{(1-h)^2(1+2x-x^2) - 8x^2}}{(1-h)^2+4}, \quad (94)$$

$$y(x) = \frac{1-h}{2}[1-t(x)] - x, \quad D = \left[0; \frac{2(1-h)^2}{(1-h)^2+4} \right],$$

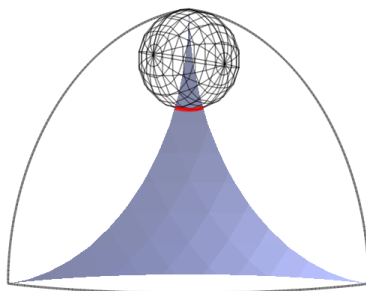


Figure 10: The intersection (in red) of octahedral face and horosphere.

one has that

$$w(h) \equiv 2 \int_D \frac{\sqrt{1 + [y'(x)]^2 + [t'(x)]^2}}{1 - x^2 - y^2(x) - t^2(x)} dx = \sqrt{2} \frac{1 - h}{1 + h}. \quad (95)$$

References

- [1] W.P. Thurston, The geometry and topology of 3-manifolds. *Princeton University Lecture Notes* (1978).
- [2] N. Wielenberg, The structure of certain subgroups of the Picard group. *Math. Proc. Camb. Phil. Soc.* **84**, 427 (1978).
- [3] K. Matsumoto, Automorphic functions with respect to the fundamental group of the complement of the Borromean rings. *J. Math. Sci. Univ. Tokyo* **13**, 1–11 (2006).
- [4] R. Abe and I.R. Aitchison, Geometry and Markoff’s spectrum for $\mathbb{Q}(i)$, I. *Transact. AMS* **365**(11), 6065–6102 (2013).
- [5] R.C. Penner, The decorated Teichmüller space of punctured surfaces. *Comm. Math. Phys.* **113**, 299-339 (1987).
- [6] L.H. Kauffman and S.J. Lomonaco, Quantum entanglement and topological entanglement. *New J. Phys.* **4**, 73 (2002).
- [7] M. Iqbal, N. Tantivasadakarn, R. Verresen *et al.* Non-Abelian topological order and anyons on a trapped-ion processor. *Nature* **626**, 505–511 (2024).
- [8] T. Kraemer, M. Mark, P. Waldburger *et al.* Evidence for Efimov quantum states in an ultracold gas of caesium atoms. *Nature* **440**, 315–318 (2006).
- [9] E. Braaten and H.-W. Hammer, Universality in few-body systems with large scattering length. *Phys. Rep.* **428**, 259-390 (2006).
- [10] K.S. Chichak *et al.* Molecular Borromean Rings. *Science* **304**, 1308-1312 (2004).
- [11] C. Rovelli and F. Vidotto, In: *Covariant Loop Quantum Gravity: An Elementary Introduction to Quantum Gravity and Spinfoam Theory* (Cambridge University Press, Cambridge, 2014).
- [12] C. Kassel, *Quantum groups* (Springer-Verlag, New York, 1995).

- [13] D.A. Tomalia, J.B. Christensen and U. Boas, *Dendrimers, Dendrons and Dendritic Polymers. Discovery, Applications and the Future* (Cambridge University Press, Cambridge, 2012).
- [14] J. Feder, *Fractals* (Plenum Press, New York, 1988).
- [15] A.I. Bobenko, U. Pinkall, and B.A. Springborn, Discrete conformal maps and ideal hyperbolic polyhedra. *Geom. Topol.* **19**, 2155-2215 (2015).
- [16] X.D. Gu, F. Luo, J. Sun, and T. Wu, A discrete uniformization theorem for polyhedral surfaces. *J. Differential Geom.* **109**, 223-256 (2018).
- [17] N. Manton and P. Sutcliffe, *Topological Solitons* (Cambridge University Press, Cambridge, 2004).
- [18] A. Nazarenko, Time level splitting in quantum Chern–Simons gravity. *Class. Quantum Grav.* **22**, 2107-2120 (2005).
- [19] A.V. Nazarenko, Area quantization of the parameter space of Riemann surface in genus two. *Ukr. J. Phys.* **58**, 1055-1064 (2013).
- [20] N.E. Hurt, *Geometric Quantization in Action: Applications of Harmonic Analysis in Quantum Statistical Mechanics and Quantum Field Theory* (D. Reidel Publishing Company, 1983).
- [21] K. Matsumoto, H. Nishi, and M. Yoshida, Automorphic functions for the Whitehead-link-complement group. *Kyushu University Preprint Series in Mathematics* (2005).
- [22] O. Rodrigues, *Journal de Mathématiques Pures et Appliquées de Liouville* **5**, 380–440 (1840).
- [23] G. Higman, B.H. Neumann, and H. Neumann, Embedding theorems for groups. *J. London Math. Soc.* **24**, 247–254 (1949).
- [24] J.B. Wilker, The quaternion formalism for Möbius groups in four or fewer dimensions. *Lin. Alg. Appl.* **190**, 99-136 (1993).
- [25] C. Adams, A. Calderon, and N. Mayer, Generalized bipyramids and hyperbolic volumes of alternating k -uniform tiling links. *Topol. Appl.* **271**, 107045 (2020).
- [26] J.G. Ratcliffe and S.T. Tschantz, Cusp transitivity in hyperbolic 3-manifolds. *Geom. Dedicata* **212**, 141–152 (2021).
- [27] N.R. Hoffman, Cusp types of quotients of hyperbolic knot complements. *Proc. Amer. Math. Soc. Ser. B* **9**, 336-350 (2022).
- [28] A.V. Nazarenko, Directed random walk on the lattices of genus two. *Int. J. Mod. Phys. B* **25**, 3415–3433 (2011).
- [29] O. Knill, *Probability and stochastic processes with applications* (Overseas Press, New Delhi, 2009).
- [30] M. Abramowitz and I.A. Stegun (eds), *Handbook of mathematical functions with formulas, graphs, and mathematical tables* (Dover Publications, New York, 1972).
- [31] A. Papadopoulos and S. Yamada, Deforming hyperbolic hexagons with applications to the arc and the Thurston metrics on Teichmüller spaces. *Monatsh. Math.* **182**, 913–939 (2017).

- [32] C.T. McMullen, Braid groups and Hodge theory. *Math. Ann.* **355**, 893–946 (2013).
- [33] B. Farb and D. Margalit, *A Primer on Mapping Class Groups* (Princeton University Press, Princeton, 2012).
- [34] S. Albeverio and S. Rabanovich, On a class of unitary representations of the braid groups B_3 and B_4 . *Bul. Sci. Math.* **153**, 35–56 (2019).
- [35] S. Albeverio and A. Kosyak, q -Pascal’s triangle and irreducible representations of the braid group B_3 in arbitrary dimension. ArXiv: 0803.2778 [math.QA].
- [36] C. Rovelli and L. Smolin, Discreteness of area and volume in quantum gravity. *Nucl. Phys. B* **442**, 593–619 (1995).
- [37] F. Luo, Rigidity of polyhedral surfaces, I. *J. Differential Geom.* **96**, 241–302 (2014).